PCCP

ROYAL SOCIETY OF CHEMISTRY

PAPER

View Article Online
View Journal | View Issue

Cite this: *Phys. Chem. Chem. Phys.*, 2020, **22**, 10149

Penning spectroscopy and structure of acetylene oligomers in He nanodroplets

S. Mandal,[a] R. Gopal,[b] M. Shcherbinin,[c] A. D'Elia,[d] H. Srinivas,[e] R. Richter,[f] M. Coreno,[fg] B. Bapat,[a] M. Mudrich,[ch] S. R. Krishnan*[h] and V. Sharma*[i]

Received 7th February 2020,
Accepted 20th April 2020

DOI: 10.1039/d0cp00689k

rsc.li/pccp

Embedded atoms or molecules in a photoexcited He nanodroplet are well-known to be ionized through inter-atomic relaxation in a Penning process. In this work, we investigate the Penning ionization of acetylene oligomers occurring from the photoexcitation bands of He nanodroplets. In close analogy to conventional Penning electron spectroscopy by thermal atomic collisions, the n = 2 photoexcitation band plays the role of the metastable atomic 1s2s ^{3,1}S He*. This facilitates electron spectroscopy of acetylene aggregates in the sub-Kelvin He environment, providing the following insight into their structure: the molecules in the dopant cluster are loosely bound van der Waals complexes rather than forming covalent compounds. In addition, this work reveals a Penning process stemming from the n = 4 band where charge-transfer from autoionized He in the droplets is known to be the dominant relaxation channel. This allows for excited states of the remnant dopant oligomer Penning-ions to be studied. Hence, we demonstrate Penning ionization electron spectroscopy of doped droplets as an effective technique for investigating dopant oligomers which are easily formed by attachment to the host cluster.

1 Introduction

He nanodroplets have been regarded as an ideal host environment for spectroscopic studies of embedded atoms and molecules over a vast spectral range spanning from the infrared to the vacuum ultraviolet due to their ability to ro-vibronically cool these dopants without any chemical modification. However, this seemingly passive He host environment proves to be fertile ground for studying a rich class of intermolecular relaxation processes between the excited host and the attached dopants when being photoexcited.[1–3] A potent observable for obtaining insights into these processes is the energy distribution of ejected electrons tagged to particular ions arising out of these multi-atomic processes. This observable can be applied specifically to study the indirect Penning ionization of dopant aggregates interacting with photoexcited He* in the droplets whereby the participating quantum states of both the embedded species and the droplets can be discerned. Although a recent report[4] suggested that the scattering of electrons following Penning ionization may obscure the molecular features, we were able to resolve the Penning ionization electron spectra (PIES) in the case of acetylene (C_2H_2) oligomers. This motivates the development of ion-correlated energy-resolved electron detection in combination with the Penning process as a spectroscopic tool to study the electronic structure of weakly-bound quantum aggregates. These atomic and molecular complexes can be aggregated with relative ease by employing He nanodroplets as a nanoscale sub-Kelvin container.[5–7] The application of Penning spectroscopy aided by coincident electron–ion detection to small acetylene clusters in nanodroplets indicates a loosely bound van der Waals aggregate of C_2H_2 molecules in the sub-Kelvin He nanodroplet environment.

Our investigation includes a series of electron–ion coincidence measurements detailed in the next section. Aided with information about the prominent fragmentation products through 20–26 eV photon energy, the kinetic energy distributions of electrons in coincidence with these ions are measured. To initiate the Penning ionization we choose 21.6 eV photoexcitation corresponding to the most important n = 2 droplet band. Typically, doped alkali atoms which reside on the droplet surface are known to be preferentially Penning ionized by this excitation of the complex.[1,8] Here, we measured electron kinetic energy spectra in coincidence with the most abundant dopant cluster ions, $C_2H_2^+$, $[C_2H_2]_2^+$ and $[C_2H_2]_3^+$. In contrast to studies hitherto,[1] we were also able to use the autoionizing n = 4 droplet band for PIES of

[a] *Indian Institute of Science Education and Research, Pune 411008, India*
[b] *Tata Institute of Fundamental Research, Hyderabad 500107, India*
[c] *Aarhus University, 8000 Aarhus C, Denmark*
[d] *Department of Physics, University of Trieste, Via A. Valerio 2, 34127 Trieste, Italy*
[e] *Max-Planck-Institut für Kernphysik, 69117 Heidelberg, Germany*
[f] *Elettra-Sincrotrone Trieste, 34149 Basovizza, Italy*
[g] *Consiglio Nazionale delle Ricerche – Istituto di Struttura della Materia, 34149 Trieste, Italy*
[h] *Indian Institute of Technology Madras, Chennai 600036, India. E-mail: srkrishnan@iitm.ac.in*
[i] *Indian Institute of Technology Hyderabad, Kandi 502285, India. E-mail: vsharma@iith.ac.in*

acetylene doped He nanodroplets which can reveal acetylene cluster ions left in excited states higher than those possible in the case of the $n = 2$ excitation. Not only does PIES reveal details about the dopant oligomers, the converse, the relaxation behavior of excited He* in the droplet containing the dopant is also a subject of current studies. The He droplet is expected to internally relax from the dipole allowed 1s2p ^{1}P to 1s2s ^{3,1}S He* states before the Penning ionization ensues.[9–11]

This work on the Penning ionization of acetylene oligomers mediated by different photo-excitation bands of He nanodroplets is revealing in many respects:

First, we gain insights in the relaxation dynamics of excited He nanodroplets and in the electronic states of acetylene oligomers involved in the Penning ionization process. In addition to the $n = 2$ states of He*, higher states of He* are found to induce Penning ionization of acetylene thereby accessing higher-lying states of the acetylene product ion.

Second, PIES reveals a dominant monomer-like feature even for Penning electrons tagged to the acetylene dimer and trimer ions pointing to a weakly bound van der Waals system of the aggregate inside the droplet. This is reminiscent of the foam-like structure evidenced in the case of Mg doped into He nanodroplets.[6]

2 Experimental details

Our investigations are the result of a beamtime at the Gas-Phase (GAPH) beamline at the Elettra Synchrotron Trieste, Italy. The schematic of the experiment is depicted in Fig. 1 while the details have been presented elsewhere.[1,4,12,13] In brief, the implementation consists of three sections. The first one is the source chamber where He nanodroplets are generated by supersonic expansion from a cryogenically cooled nozzle. This is attached to a doping chamber where the droplet jet picks up dopant molecules from the doping chamber. The stream of doped droplets then enters the interaction chamber where the doped droplets are intercepted by the synchrotron radiation. To produce He nanodroplets, in the source chamber pressurized ($\sim$50 bar) high-purity helium gas (He 6.0) is supersonically expanded through a cryogenically cooled nozzle with a 5.0 μm orifice. The jet is extracted using a trumpet-shaped skimmer with a 0.4 mm aperture. The variation of the nozzle temperature (T_{noz}) serves to control the mean size of the droplets; typically varying T_{noz} between 16 and 14 K allows a control of droplet sizes between 8800 and 23 000 He atoms per droplet on the average.[14,15]

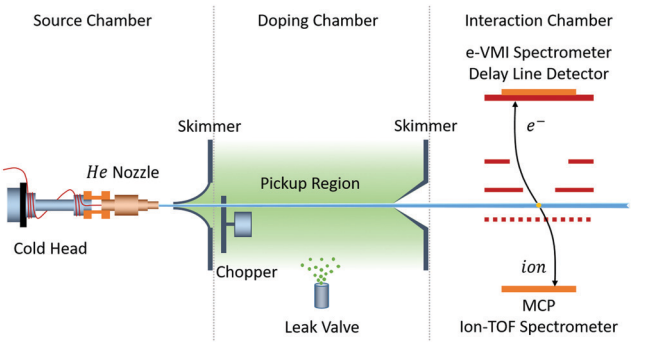

Fig. 1 Schematic diagram of the experimental setup. He droplets are generated in the source chamber by supersonic expansion of the He gas through the cryogenic nozzle and extracted into the next region by a skimmer. The jet of droplets is doped by picking up C_2H_2 molecules which are effused in the doping chamber downstream. Subsequently, in the interaction chamber, the doped He droplet jet is ionized by EUV synchrotron radiation. The resultant electrons and ions are measured in coincidence by the VMI and TOF spectrometers operating in tandem.

The skimmed jet of He nanodroplets exits the source chamber to pick up C_2H_2 molecules which were effused into the doping chamber by a controlled leak through a dosing valve. This variation of the partial acetylene pressure (P_d) in this region, 6×10^{-7} mbar to 4×10^{-6} mbar, offers a direct control over the pick up of the dopant molecules which follows Poissonian statistics. The number of dopant molecules per droplet can be varied between at the most one dopant molecule per droplet, to several molecules captured into a typical droplet in the jet. Before doping, it is important to distil acetylene gas to remove inevitable acetone contamination. We passed the precursor through a coiled copper tube immersed in a bath with ethanol and liquid N_2 slurry maintained at 173 K. Furthermore, a mechanical chopper operating between the source and the doping chambers to periodically intercept the nanodroplet jet enables us to record distinct background signals arising out of the effusive residual gas molecules in addition to acquiring signals from doped droplets. These measurements performed in quick succession, typically switching at $\sim$70 Hz, allow us to reliably subtract the background due to effusive gases enabling low-noise acquisition of droplet specific signals.

Downstream of the doping chamber, the doped droplet jet passes through a second skimmer to enter into the interaction chamber (*cf.* Fig. 1). This chamber, maintained at $\sim 10^{-8}$ mbar houses a velocity map imaging (VMI) spectrometer for electrons along with a time-of-flight (TOF) spectrometer for ions operating in tandem. At the geometric center of the interaction chamber the doped droplets interact with the focused beam of linearly polarized EUV photons from the synchrotron. The photon beam has a typical peak intensity of $\sim$15 W m^{-2} at a repetition rate of 500 MHz in the form of $\sim$150 ps pulses. We have used photon energies between 20 and 26 eV for electronic excitation and ionization of the host He matrix. Two slits in the photon beam path were adjusted to maintain moderate count-rates in the range of 10–20 kHz on the charged particle detectors. To suppress the higher order harmonics of the synchrotron radiation, a Sn filter was used for measurements at 21.6 eV photon energy. The beamline is capable of a resolving power of $\Delta E/E \leq 10^{-4}$ over the whole photon energy range.

The VMI and TOF spectrometers operating synchronously in the interaction chamber enable electron–ion coincidence measurements. Both the single and double ion coincidences with electrons were implemented in these experiments. From sufficiently long acquisitions, time-of-flight ion–ion correlation maps were obtained along with the corresponding electron-VMI distributions. However, these ion–ion coincidence maps did not evidence any double ionization of C_2H_2 doped He nanodroplets in the studied photon energy range. The kinetic energy distributions

of the electrons are derived from the velocity-map-images recorded on a position sensitive delay-line detector of the VMI spectrometer. These were Abel inverted using well-established protocols – we employed B. Dick's MEVELER[16] for inversion. To calibrate the kinetic energy of electrons for a given configuration of the VMI spectrometer, we referenced photoionization of atomic He over a few photon energies in the range of 25 eV to 40 eV. The average energy resolution ($\Delta E/E$) of the VMI spectrometer is typically ~7%. The resolution for the electron energy spectra shown here is limited by the resolution of the VMI spectrometer. The TOF spectra of ions were correlated to electron energy spectra obtained from the VMI.

3 Results and discussion

3.1 Ion yield

Droplet induced ionization of doped acetylene can be readily observed by recording the ion yield of $C_2H_2^+$ as a function of photon energy in the energy range from 20 eV to 26 eV (*cf.* Fig. 2). Fig. 2 also shows the measured He_2^+ yield from doped droplets in the same photon energy range for comparison as this is known to be the most prominent ion arising out of the host. This reveals two important aspects of the induced ionization of acetylene doped droplets. The feature at the $n = 2$ droplet band centered at 21.6 eV where only dopant $C_2H_2^+$ ions (red) are seen without any significant yield of He_2^+ is characteristic of the Penning process. At higher photon energies, beyond the autoionization threshold (~23 eV) of pure He droplets, both $C_2H_2^+$ and He_2^+ yields follow very similar trends.

It is well known that, at a photon energy of 21.6 eV, there is a very high cross section for the droplet to photoexcite to the $n = 2$ band derived from the 1s2p atomic He level.[17] Following this photoexcitation, due to repulsive interaction with the droplet environment, the excited He* usually migrates to the surface of the droplet and Penning ionization is found to be particularly efficient for surface-bound alkali atoms.[1] However, more recently, Penning ionization of immersed molecules was also clearly observed.[4] As we observe a peak in the $C_2H_2^+$ yield from the droplet at the same photon energy, we expect the doped acetylene molecules, which are believed to stay at the interior of the droplet, to be ionized by the following Penning process:

$$\begin{aligned} He_m + [C_2H_2]_n + h\nu &\rightarrow He_m^* + [C_2H_2]_n \\ &\rightarrow He_m + [C_2H_2]_n^+ + e_{Penning}^- \end{aligned} \quad (1)$$

The peak structures below the ionization energy of atomic He (E_i^{He} = 24.58 eV) in the He_2^+ yield correspond to the autoionization of the He nanodroplets. This occurs *via* droplet photoexcitation to Rydberg states of He_2* which are derived from atomic 1s*n*p ^{1}P, $n > 2$ states ($23\ eV < h\nu < E_i^{He}$). For $h\nu \geq E_i^{He}$, direct ionization of He atoms in the nanodroplets occurs. Common to both these ionization regimes, the He^+ or He_2^+ ion formed in the droplet usually migrates to its interior due to the net attractive interaction with the rest of the droplet enabled by fast charge hopping.[18] In the case of rare gas dopants, which reside in the droplet interior, ionization by charge-transfer is the dominant dopant ionization process.[1] Thus, both these regimes, autoionization and direct ionization, are expected to contribute to dopant ionization. This is convincingly evidenced by the yield of $C_2H_2^+$ ions following the trend of the host He_2^+ ion for $h\nu > 23$ eV, *cf.* Fig. 2, due to a charge-transfer process:

$$\begin{aligned} He_m + [C_2H_2]_n + h\nu &\rightarrow He_m^+ + [C_2H_2]_n + e_{He}^- \\ &\rightarrow He_m + [C_2H_2]_n^+ + e_{He}^-. \end{aligned} \quad (2)$$

However, in the autoionization regime ($23\ eV < h\nu < E_i^{He}$), previous studies with Li and Ar doped He nanodroplets reported significantly low contributions of Penning ionization from He* (1s2s) excited states which competes with the dominant charge-transfer channel.[1] Further, in comparison to the He* 1s2s states, the contribution to dopant Penning ionization from higher excited states He* (1s*n*p, $n > 2$) in Li doped droplets is rather small.[10] The energy distributions of the emitted electrons measured in coincidence with ions for both the Penning (1) and charge-transfer (2) ionization processes are expected to be distinct. The corresponding electron spectra would also enable the identifications of the ionization processes and of the participating electronic states corresponding to the doped C_2H_2 oligomer and the He host.

Fig. 3 shows the ion mass spectra at two different photon energies: (a) 21.6 eV and (b) 23.9 eV, where the red curve corresponds to the ionization of residual background gases and the green curve is the signal from droplet ionization in addition to the background. The ion mass spectra are normalized such that the background N_2^+ yields are proportional to the photoionization cross sections of N_2 for producing N_2^+ at the respective photon energies.[19] We observe acetylene oligomer ions including

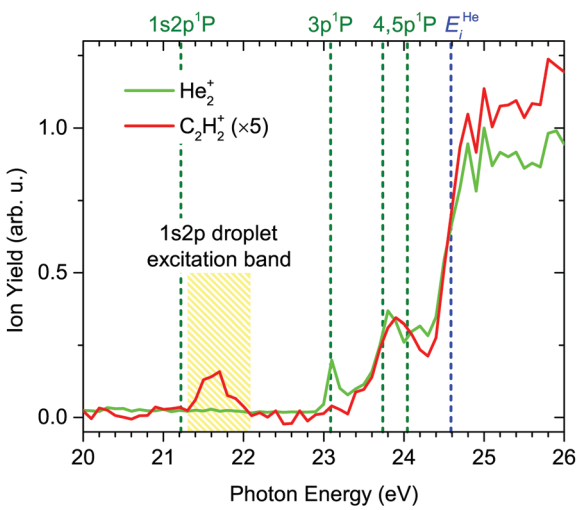

Fig. 2 Ion yields of He_2^+ and $C_2H_2^+$ from the acetylene doped He droplet as function of photon energy. The nozzle temperature and doping chamber pressure are maintained at 16 K and 6.5 × 10^{-7} mbar, respectively. The blue vertical dashed line represents the ionization energy of atomic He (E_i^{He}) and the vertical green dashed lines at 21.21 eV, 23.09 eV, 23.78 eV, and 24.04 eV represent atomic He* 1s2p ^{1}P, 1s3p ^{1}P, 1s4p ^{1}P and 1s5p ^{1}P energy levels, respectively. The yellow shaded region shows the droplet photoexcitation band correlated to the 1s2p atomic He level.

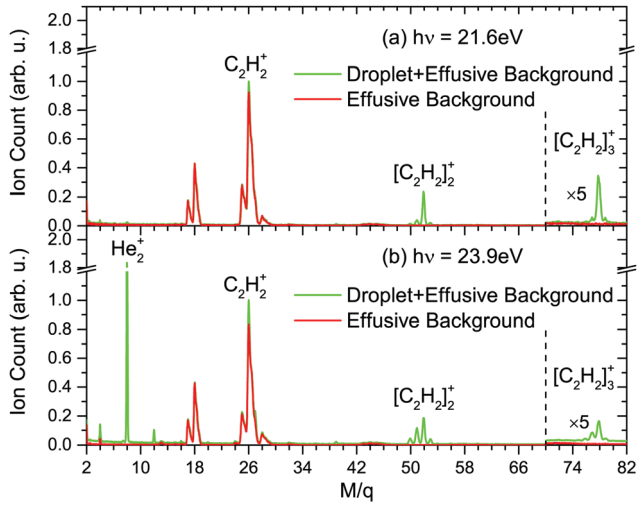

Fig. 3 Ion mass spectra at photon energies of (a) 21.6 eV, and (b) 23.9 eV for T_{noz} = 14 K and P_d = 4.5 × 10^{-6} mbar. The green line represents the droplet and effusive background signal and red line represents only the effusive background signal. The horizontal axis shows the mass (M) to charge (q) ratio of the ionic fragments.

the monomer ($C_2H_2^+$), the dimer ($[C_2H_2]_2^+$) and the trimer ($[C_2H_2]_3^+$) from doped droplets. At 23.9 eV, we also observe He cluster ions (He_m^+, m = 1–3) originating from droplet autoionization. We also observe more extensive fragmentation of acetylene oligomer ions around the corresponding dimer and trimer ion peaks at this photon energy which is significantly different from the Penning ionization at $h\nu$ = 21.6 eV. The fragmentation we observe in the charge-transfer process occurring in the droplet is reminiscent of that reported in the case of a similar process in thermal collisions of He^+ ions with C_2H_2 molecule.[20]

In the Penning ionization process, at $h\nu$ = 21.6 eV, acetylene dimer and trimer ions along with their fragments were detected from droplet ionization. But the yield of monomer $C_2H_2^+$ ions with significant contrast of droplet specific signal over residual gas background was extremely low. Both for single doping (P_d = 6.5 × 10^{-7} mbar) and for conditions optimized to multiply dope the He droplet with C_2H_2 molecules with relatively high acetylene pressures (P_d = 4.5 × 10^{-6} mbar) in the doping chamber, the signal of droplet specific monomer $C_2H_2^+$ ions was low. Note that, even for the multiple doping condition, when the partial pressure of C_2H_2 is high inside the doping chamber, only C_2H_2 monomers are present in high density in the doping chamber. This is evident from the residual background ion signal where only the C_2H_2 monomer ion and its ionic fragments are observed but no dimer and trimer ion signals. Therefore, individual C_2H_2 molecules are picked up by the droplet, and C_2H_2 clusters are formed only inside the droplet. We ascribe two reasons for the low detection of C_2H_2 monomer ions compared to C_2H_2 oligomer ions in this Penning ionization process: (a) suppression of the escape of the smaller ion ($C_2H_2^+$) from the droplet following the Penning ionization; (b) in the case of multiply doped droplets, the formation of larger oligomer ions by the association of first Penning ionized $C_2H_2^+$ with other doped neutral C_2H_2 molecules in the droplet. We will discuss this further in the context of the PIES in the next section. The energy released in the association process evaporates several He atoms from the droplet leading to a disintegration of the complex which enables the escape and eventual detection of C_2H_2 oligomer ions.

3.2 Electron energy spectra

3.2.1 At n = 2 droplet excitation band. Previous studies on rare-gas (Xe, Kr) doped He nanodroplets by Wang *et al.*,[9] and on acene doped droplets by Shcherbinin *et al.*[4] reported PIES correlated to the dopant ions upon photoexcitation to the n = 2 droplet excitation band. In both cases, the Penning electrons undergo inelastic scattering with the surrounding He environment and significantly lose energy which leads to a broad low-energy feature in the PIES. While for Xe and Kr doped droplets the PIES retain some features of unperturbed Penning electrons, for acene doped droplet the reported PIES are massively perturbed by the He environment and thereby no information about the participating acene and He* states in the Penning process are gained.

Interestingly, from our experiment with C_2H_2 doped droplets, we are able to gain insight into the electronic structure of the dopant cluster as well as about the relaxation dynamics of the He* from the measured PIES in coincidence with the Penning ions. Fig. 4 presents the PIES correlated to (a) acetylene dimer ions ($[C_2H_2]_2^+$) and (b) acetylene trimer ions ($[C_2H_2]_3^+$) originating from dopant Penning ionization when the doped droplet is photoexcited at 21.6 eV. The measured PIES in coincidence with the dimer and trimer ions are quite similar and consist of two broad features; one in the 0.5–7.5 eV range and another in the 7.5–11 eV range.

Earlier reports, on rare gas[9] and alkali metal doped droplets,[1,10] provided evidence that upon photoexcitation at 21.6 eV, the dopants are Penning ionized not only from the He* 1s2p ^{1}P dipole excited state but also prominently from long-lived He* 1s2s ^{3}S and He* 1s2s ^{1}S states which are populated upon fast relaxation. Upon Penning ionization from these He* states, the doped C_2H_2 oligomers can be ionized to different cationic states correlated to $X^2\Pi_u$, $A^2\Sigma_g^+$, and $B^2\Sigma_u^+$ states of $C_2H_2^+$ which lie 11.4 eV, 16.7 eV, and 18.8 eV above the ground state of C_2H_2, respectively.[21] Therefore, in Fig. 4, the high energy feature (7.5–11 eV) is the result of Penning ionization of C_2H_2 oligomers to the cationic states correlated to $C_2H_2^+$ ($X^2\Pi_u$). The low-energy feature (0.5–7.5 eV) of the PIES is likely due to scattering of Penning electrons at He atoms.[9] In addition, Penning ionization of C_2H_2 oligomers to the cationic states correlated to higher excited $C_2H_2^+$ ($A^2\Sigma_g^+$, $B^2\Sigma_u^+$) may contribute.

In the indirect ionization of acetylene monomers, dimers and trimers doped into He nanodroplets, three Penning processes need to be considered:

$$He_m + [C_2H_2]_1 + h\nu \rightarrow He_m^* + [C_2H_2]_1 \rightarrow He_m + [C_2H_2]_1^+ + e_{Penning}^- \ (KE_1) \quad (3a)$$

$$He_m + [C_2H_2]_2 + h\nu \rightarrow He_m^* + [C_2H_2]_2 \rightarrow He_m + [C_2H_2]_2^+ + e_{Penning}^- \ (KE_1 + 0.96\ eV) \quad (3b)$$

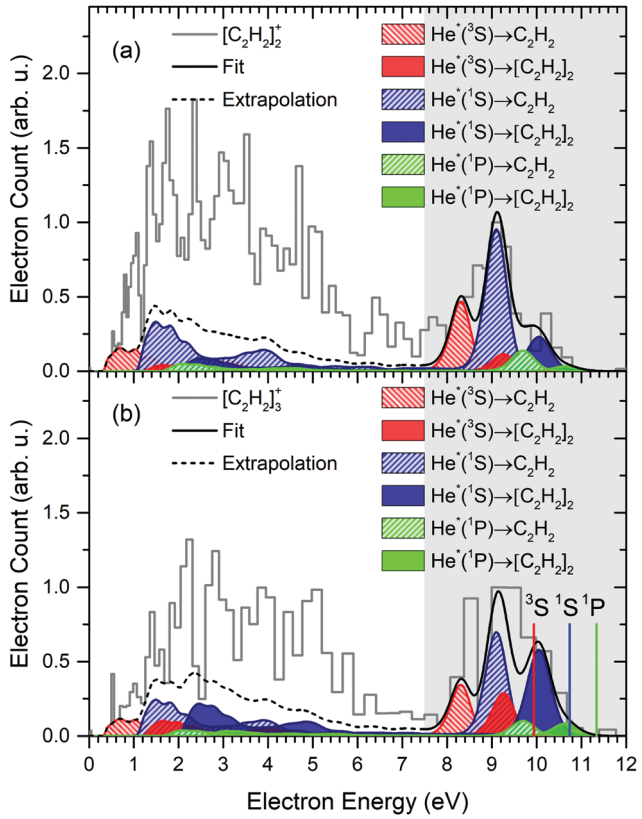

Fig. 4 PIES correlated to (a) $[C_2H_2]_2^+$ and (b) $[C_2H_2]_3^+$ from acetylene doped He droplet ionization at photon energy of 21.6 eV for P_d = 4.5 × 10^{-6} mbar and T_{noz} = 14 K. The red, blue and green spectra with hatched shading are the convoluted PIES for C_2H_2 monomer from He* 1s2s ^{3}S, 1s2s ^{1}S and 1s2p ^{1}P states, respectively, while the convoluted PIES of C_2H_2 dimer from these He* states are represented by the red, blue and green spectra with filled shading, respectively. The solid black line in each panel shows the total fit performed over the high energy feature from 7.5 eV to 11 eV which is arising from the cationic states of C_2H_2 monomer and dimer correlated to $C_2H_2^+$ $X^2\Pi_u$ state. The parameters for the fit were determined only using experimental data in the region 7.5 eV and beyond. Nonetheless, we extrapolate this using the dashed black line into the region ≤7.5 eV considering the corresponding $A^2\Sigma_g^+$ and $B^2\Sigma_u^+$ states. In panel (b), the red, blue and green vertical lines denote the PIES peak positions of C_2H_2 trimer Penning ionization from He* 1s2s ^{3}S, 1s2s ^{1}S and 1s2p ^{1}P states, respectively. Note that the width of the bar in the histogram indicates the bin size on the energy scale and does not represent the energy resolution of the VMI spectrometer.

$$He_m + [C_2H_2]_3 + h\nu \rightarrow He_m^* + [C_2H_2]_3 \rightarrow He_m + [C_2H_2]_3^+ + e_{Penning}^- \ (KE_1 + 1.57\ eV) \quad (3c)$$

3.2.1.1 Fitting procedure. In order to interpret the measured PIES correlated to acetylene dimer and trimer ions using PIES arising out of all the He* states, we use the following strategy. We rely on the earlier study by Ohno *et al.*[22] on the Penning ionization of C_2H_2 by metastable He* (1s2s ^{3}S) in slow atomic collisions and the reported PIES arising out of the Penning process. Furthermore, in order to obtain the PIES of the acetylene monomer due to Penning ionization from He* in the 1s2s ^{1}S and the dipole allowed 1s2p ^{1}P states, it is necessary to shift the reported PIES[22] by the corresponding energy differences between the He* 1s2s ^{3}S and 1s2s ^{1}S states which is +0.8 eV; similarly the shift pertaining to the He* 1s2s ^{3}S and 1s2p ^{1}P states is +1.4 eV. The relative amplitudes of the three spectral features (^{3}S, ^{1}S, ^{1}P) are obtained by fitting the experimental data of the high-energy feature (≥7.5 eV, shaded in grey in Fig. 4) of the measured PIES. The finite energy resolution of the VMI spectrometer is accounted for by convoluting these peaks in the PIES with the instrument function of the spectrometer. The lower energy part of the spectrum, 0.5–7.5 eV, unshaded region in Fig. 4, is not used in the fitting process explicitly, nor does it influence the relative amplitudes of spectral features of the Penning ionization.

Next, in order to fit the C_2H_2 dimer PIES consistent with that of the monomer we do the following: noting that the ionization threshold of C_2H_2 dimer lies 0.96 eV below the ionization threshold of its monomer,[23] the positions of the three Penning spectral peaks corresponding to ^{3}S, ^{1}S, and ^{1}P in the high-energy part (≥7.5 eV) of the PIES of the C_2H_2 dimer are obtained by shifting the corresponding peaks of the monomer by this difference in the ionization energy. Further, we also retain the relative amplitudes of these components in the fitting of the dimer to those obtained from the monomer fit. In order to obtain the fit in the high-energy part (≥7.5 eV) of the dimer PIES, the grey-shaded region in Fig. 4a, we use a set of six peaks corresponding to the Penning ionization of C_2H_2 and $[C_2H_2]_2$ arising from the set of three participating He* states (^{3}S, ^{1}S, ^{1}P). These are color coded as red, blue and green, respectively. The hatched-fill and solid-fill correspond to the monomer and dimer Penning ionization channels, respectively. A similar procedure is employed for the PIES of the C_2H_2 trimer in the droplet. We will discuss this further in a subsequent section.

However, for the broad low-energy feature in PIES, ≤7.5 eV, no attempt is made to fit this section of the spectrum. We realize from well-established phenomenology that this feature arises from electron-He scattering processes.[4,9] Therefore, we merely extended the Penning ionization curves obtained from the high energy (≥7.5 eV) part to include the A and B excited molecular states. The shaded regions under the experimental data histogram in panels (a) and (b) of Fig. 4 in the low energy part, ≤7.5 eV, capture this contribution which is consistent with the remainder of the electron kinetic energy spectra. We discuss this further, see below.

3.2.1.2 Interpretation and discussion. The high energy feature (≥7.5 eV) correlated to the $[C_2H_2]_2^+$ ion (*cf.* Fig. 4a) fits quite nicely to the modeled sum of PIES of the acetylene monomer and dimer. We discuss the novel findings in this regard first. The contribution of the 1s2s ^{3}S state of He* to the experimental PIES is relatively large (∼28%) compared to previous findings.[10] While the 1s2s ^{3}S state is not expected to be efficiently populated by droplet-induced relaxation, other factors may enhance the corresponding measured electron signal in the PIES. The Penning ionization cross-section as well as the ejection mechanism out of the droplet leading to bare $[C_2H_2]_2^+$ Penning ions also determines the amplitude of the 1s2s ^{3}S-state contribution.

The predominant contribution of this well-matched fit comes from the three channels corresponding to the Penning ionization of the acetylene monomer, described in eqn (3a) which is significantly higher than that from the ionization of the embedded dimer, process (3b). The most intriguing feature of this study is revealed by applying this procedure to the PIES correlated to $[C_2H_2]_3^+$ (*cf.* Fig. 4b). We consider the contributions of all the three processes in eqn (3a)–(3c). In considering the contributions of the Penning ionization of the monomer and dimer to the PIES, we used the same relative amplitudes of indirect ionization channels from He* (1s2s ^{3}S, 1s2s ^{1}S, and 1s2p ^{1}P) states obtained from the model-fitting of the $[C_2H_2]_2^+$ PIES using processes (3a) and (3b). We note that the ionization energy of the acetylene trimer measured in free-jet clusters is 1.57 eV lower than that of the monomer.[24] The three vertical lines in red, blue and green in Fig. 4b are the peak positions expected from the Penning ionization of the C_2H_2 trimer from He* (1s2s ^{3}S, 1s2s ^{1}S, and 1s2p ^{1}P) states, respectively. Despite this, the PIES observed in correlation to the trimer ion has a major contribution at kinetic energies lower than expected from process (3c) (red stick $\sim$10 eV in Fig. 4b), but has no significant contribution corresponding to the direct Penning ionization of the trimer especially from the singlet ^{1}S channel (blue stick $\sim$10.8 eV in Fig. 4b) which is otherwise important. Also, there is no observable electron signal at kinetic energies corresponding to the ^{1}P channel in the Penning ionization of trimers (*cf.* green stick $\sim$11.4 eV in Fig. 4b). This is, indeed, an unexpected finding which requires looking beyond the picture of Penning ionization of embedded dopant clusters hosted in He nanodroplets accepted hitherto. Rationalizing our observations necessitates incorporating the contributions of processes (3a) and (3b) in the Penning ionization of the trimers as important factors.

The ratios of dimer (3b) to monomer (3a) ionization channels for the PIES correlated to $[C_2H_2]_3^+$ and $[C_2H_2]_2^+$ are 0.92 and 0.27, respectively. In both cases, the major contributions to Penning ionization are from the monomer rather than from larger oligomers. This leads to the following picture: acetylene molecules may not form a covalently bound trimer in He nanodroplets. Instead the aggregate is very likely loosely bound retaining significant characteristics of the electronic structure of the monomer. This finding is in line with recent results from an infrared spectroscopic study of acetylene dimers in He nanodroplets.[25] Nonetheless, the unambiguous observation of the oligomer ions leads us to the conclusion that following the Penning ionization, the oligomer ions are strongly bound and escape the droplet facilitated by the energy released into the droplet. The free jet study indicates that the $[C_2H_2]_2^+$ and $[C_2H_2]_3^+$ are covalently bound with substantial binding energies $>$2 eV.[26] This unusual behavior of acetylene oligomers in the droplet is reminiscent of the foam-like structure of the dopant aggregate in Mg-doped He nanodroplets[6] and state-specific spatial separation observed in (Cr)-dimers in He nanodroplets.[27] Furthering the analogy, the Mg-foam was also observed to collapse upon photoexcitation forming strongly bound oligomers in the excited state. This should motivate further experimental and theoretical investigations of the spatial and electronic structures of mesoscopic aggregates formed inside this quantum fluid host.

In the remainder of this article, we discuss the low-energy feature (0.5–7.5 eV) in the PIES at 21.6 eV photon energy (*cf.* Fig. 4) as well as indirect dopant ionization in the autoionization regime. The interpretation of similar broad low-energy features as observed in previous studies,[4,9] was due to the inelastic scattering of the Penning electrons with the surrounding He environment and due to possible interaction with the electron bubble states in the droplet.[28] We account for the scattering effects on the Penning electrons in the droplet by performing a Monte Carlo simulation based on binary electron-He scattering, similar to the work on acene doped droplet.[4] However, despite incorporating all the features of electron-He scattering in our simulations, we found that even for a large droplet radius of 30 nm (compared to 6.5 nm in our experiments for T_{noz} = 14 K and He expansion pressure of 50 bar) the simulated PIES do not agree with the low-energy part of the electron energy spectra. This indicates that one should take into account possible electron bubble interactions in the simulation. This low-energy feature also arises from the higher excited A and B states of $C_2H_2^+$. The large Penning ionization signal involving the A and B states as compared to that in earlier molecular beam experiments[22] may be related to the steep dependence of the corresponding effective cross-sections on the collision energy.[29]

3.2.2 At *n* = 4 droplet excitation band. To learn about the ionization mechanisms in the autoionization regime (23 eV $< h\nu <$ E_i^{He}), we photoexcited the doped droplet across the n = 4 droplet band corresponding to the atomic He* (1s4p ^{1}P) excitation. The electron spectra correlated to He_2^+, $C_2H_2^+$ and $[C_2H_2]_2^+$ are presented in Fig. 5 at two different photon energies, 23.9 eV where a pronounced ionization maximum was observed, and 24.3 eV which is a minimum that follows in Fig. 2.

The electron spectra correlated to He_2^+ at both photon energies (*cf.* Fig. 5a1 and a2) reveal very low-energy ($\sim$100–500 meV) electrons which are the signature of He nanodroplet autoionization.[30] Interestingly, the electron spectra correlated to $C_2H_2^+$ and $[C_2H_2]_2^+$ (*cf.* Fig. 5b1, b2, c1 and c2) at 23.9 eV and 24.3 eV photon energies also show similar low energy features although these are broader with their maxima shifted to higher energies as compared to that of He_2^+. This indicates that conventional charge-transfer from the He_2^+ in the droplet formed due to autoionization (2) cannot be the only mechanism for the formation of the acetylene oligomer ions. The additional low energy peak around 0.5 eV could therefore be due to Penning ionization of C_2H_2, leading to highly excited $C_2H_2^+$. We measured photoelectron spectra (PES) from effusive C_2H_2 molecule at the two relevant photon energies (*cf.* Fig. 5d1 and d2). Simulated PES from the higher-lying $C^2\Sigma_g^+$ and $D^2\Sigma_u^+$ states of $C_2H_2^+$ whose ionization energies are 23.33 eV and 23.53 eV,[31] respectively, fit the observed PES quite well.

To confirm the additional Penning ionization of acetylene from 1s4p ^{1}P state of He* resulting in $C_2H_2^+$ in $C^2\Sigma_g^+$ and $D^2\Sigma_u^+$ states, we used the following two-function fitting procedure to analyse the electron spectra correlated to $C_2H_2^+$ and $[C_2H_2]_2^+$ from droplet ionization:

$$F(E) = \frac{C^{MB}}{(k_B T)^{3/2}}\sqrt{E}e^{-\frac{E}{k_B T}} + \sum_{i=1,2}\frac{C_i^G}{\sigma}e^{-\frac{\left(E-E_i^p\right)^2}{2\sigma^2}}$$

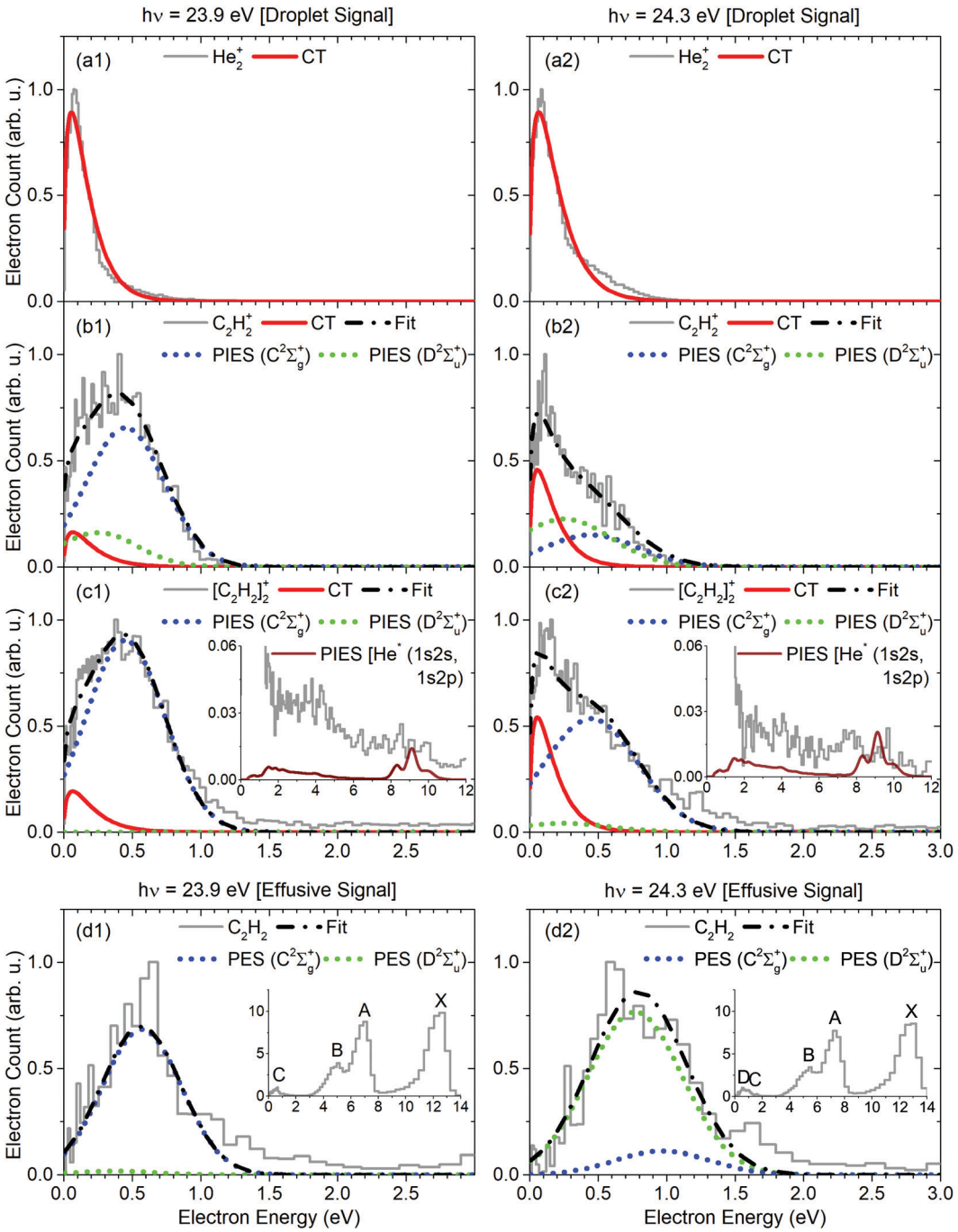

Fig. 5 Electron energy spectra at two photon energies, (1) 23.9 eV and (2) 24.3 eV, correlated to different ions (a1 and a2) He_2^+, (b1 and b2) $C_2H_2^+$, (c1 and c2) $[C_2H_2]_2^+$ from the acetylene doped droplet ionization at P_d = 4.5 × 10^{-6} mbar and T_{noz} = 14 K. The conventional charge-transfer (CT) ionization processes are shown by red curves whereas the new Penning processes *via* He* (1s4p ^{1}P) state leading to $C_2H_2^+$ $C^2\Sigma_g^+$ and $D^2\Sigma_u^+$ states are shown by blue and green dotted curves respectively. Black dashed curves are the sum of CT and Penning processes. The insets in panel (c1) and (c2) show the zoomed out electron spectra correlated to $[C_2H_2]_2^+$ ion at $h\nu$ = 23.9 eV and $h\nu$ = 24.3 eV, respectively, where we can see the presence of Penning ionization channels from He* (1s2s, 1s2p) states represented by brown lines in (c1 and c2) observed at $h\nu$ = 21.6 eV. PES correlated to effusive C_2H_2 photoionization at (d1) 23.9 eV and (d2) 24.3 eV photon energies. The blue and green dotted curves represent the simulated PES from $C_2H_2^+$ $C^2\Sigma_g^+$ and $D^2\Sigma_u^+$ states, respectively. The insets in panel (d1) and (d2), PES peaks from $C_2H_2^+$ $X^2\Pi_u$, $A^2\Sigma_g^+$, $B^2\Sigma_u^+$, $C^2\Sigma_g^+$ and $D^2\Sigma_u^+$ states can be observed.

where the Maxwell–Boltzmann distribution function (first term) represents the charge-transfer ionization component and the Gaussian functions (second term) represent the new Penning ionization channels. Using the value of T, obtained from the fitting of the electron spectra in coincidence with He_2^+, we fit the electron spectra correlated to $C_2H_2^+$ and $[C_2H_2]_2^+$ varying the coefficients C^{MB} and C_i^G. Since Penning ionization could occur from atomic He* (1s4p ^{1}P), the Gaussian peak positions (E_i^p) are fixed at the energy differences between He* (1s4p ^{1}P) and $C_2H_2^+$ ($C^2\Sigma_g^+$, $D^2\Sigma_u^+$) states while the standard deviation (σ) is fixed from

the fitting of the effusive acetylene. As the energy distribution of the autoionized electrons which are detected in coincidence with He_2^+ fits the Maxwell–Boltzmann distribution quite well, we used the same Maxwell–Boltzmann distribution to fit the charge-transfer ionization component. Note that, the observed energy distribution of the autoionized electrons is relatively high compared to previous report by Peterka *et al.*[32] due to the finite energy resolution of the VMI spectrometer.

The charge-transfer components are marked by red curves whereas blue and green dotted lines represent the new Penning ionization components from $C_2H_2^+$ $C^2\Sigma_g^+$ and $D^2\Sigma_u^+$ states, respectively, in Fig. 5b1, b2, c1 and c2. Thus, we identify a prominent Penning mechanism leading to higher-lying $C^2\Sigma_g^+$ and $D^2\Sigma_u^+$ states of $C_2H_2^+$ *via* He* 1s4p ^{1}P.

Whereas at $h\nu$ = 23.9 eV the Penning channel dominates, at $h\nu$ = 24.3 eV charge-transfer ionization is more favourable. We notice that the electron spectra in coincidence with $[C_2H_2]_2^+$ at these energies (insets of Fig. 5c1 and c2) also have weak long tails, extending up to nearly 11 eV. This tail is possibly due to Penning ionization from He* 1s2s and He* 1s2p states arising from internal relaxation, as observed in PIES at $h\nu$ = 21.6 eV. Previous femtosecond pump–probe studies on pure He nanodroplets[33,34] reported that upon photoexcitation to the n = 4 droplet band, fast internal relaxation to the n = 2 droplet band on a time scale of 2–3 ps occurs. The observed strong Penning ionization signal from He* (1s4p) compared to the Penning ionization from internally relaxed n = 2 states indicates that the Penning ionization from He* (1s4p) occurs on a faster time scale than the relaxation time of the droplet.

Upon photoexcitation to the n = 2 droplet excitation band at 21.6 eV, we observed Penning ionization of acetylene clusters leading to $C_2H_2^+$ in X, A, and B states. However, when the droplet is photoexcited to even higher 1s4p state, Penning ionization channels leading to higher-lying $C_2H_2^+$ states such as C and D states become energetically accessible and are observed here in this autoionization regime along with Penning ionizations leading to lower-lying $C_2H_2^+$ states (X, A, B). The enhanced Penning ionization cross-section leading to C and D states by He* 1s4p ^{1}P could be related to the near degeneracy of these C and D states with the 1s4p ^{1}P state.

This interpretation is further supported by PIES recorded for He nanodroplets doped with Li atoms presented previously by Ben Ltaief *et al.*[10] The spectrum recorded at $h\nu$ = 21.6 eV (maximum of the 1s2p ^{1}P absorption band) is dominated by electrons emitted by Penning ionization of Li interacting with He* in the 1s2s ^{1}S and ^{3}S states. In the coincident electron energy spectra recorded above the droplet ionization threshold (23 eV), the peaks between 13 and 16 eV reflected Penning ionization of Li after electronic relaxation of the excited He droplet into the 1s2s ^{1}S and ^{3}S states,[10] and the low-intensity feature around 18 eV was due to Penning ionization involving the 1s3s; 1s3p and 1s4s; 1s4p states of He*. The fact that the contribution to the Li Penning ionization signal arising from these higher excited states is significantly lower than in the case of acetylene may be due to the differing location of the dopants in the droplet: Li atoms are on the surface, whereas C_2H_2 molecules are expected to be located in the He droplet interior. Consequently, a He* initially localized within the He droplet migrates over a significant distance until it reaches the Li dopant which affords the relaxation into the metastable 1s2s ^{1}S and ^{3}S states before Penning ionization occurs. In comparison, the distance between the He* and the acetylene dopant is shorter on average thereby facilitating direct Penning ionization prior to He* relaxation.

4 Conclusion

Scattering of electrons following the Penning ionization of dopants in He nanodroplets obscures molecular electron spectra, as demonstrated earlier in the case of acene molecules used as dopants.[4] In this work we show that this is not always the case. Penning ionization can indeed be used as spectroscopic tool to study atomic and molecular quantum aggregates formed in He nanodroplets by exciting the host matrix. By studying the electrons and ions for the host and dopant in coincidence, we identify relevant excited states of the host and the dopant. Furthermore, we demonstrate that this generic Penning ionization electron spectroscopy scheme is not limited only to the n = 2 droplet excitation but can be extended to perform spectroscopy employing higher droplet excitation bands such as n = 4 to probe the excited states of the dopant cluster *e.g.*, the C and D states in acetylene ion. Employing this technique we uncover the structure of acetylene clusters formed inside nanodroplets. They coalesce in the form of loosely bound van der Waals aggregates, akin to a foam as observed for magnesium, rather than as a covalently bound system. This structure collapses into a composite oligomer ion following Penning ionization. Our work motivates further investigation of the structure of molecular aggregates in He nanodroplets. This study establishes Penning ionization electron spectroscopy as a widely applicable technique to probe mesoscopic quantum aggregates in nanodroplets which behave like nano-cryostats even when they are photoactivated.

Conflicts of interest

There are no conflicts to declare.

Acknowledgements

VS, RG and SRK are grateful to DST, India and ICTP, Trieste, for support (proposal # 20165468) to carry out this campaign at the Elettra Synchrotron facility. VS and SRK acknowledge financial support from the IMPRINT scheme. SRK thanks the Max Planck Society for supporting this research *via* the Partner group. MM acknowledges support from the Carlsberg Foundation, and with SRK for the funding from the SPARC Programme, MHRD, India.

Notes and references

1 D. Buchta, S. R. Krishnan, N. B. Brauer, M. Drabbels, P. O'Keeffe, M. Devetta, M. Di Fraia, C. Callegari, R. Richter, M. Coreno, K. C. Prince, F. Stienkemeier, R. Moshammer and M. Mudrich, *J. Phys. Chem. A*, 2013, **117**, 4394–4403.

2 A. C. LaForge, V. Stumpf, K. Gokhberg, J. von Vangerow, F. Stienkemeier, N. V. Kryzhevoi, P. O'Keeffe, A. Ciavardini, S. R. Krishnan, M. Coreno, K. C. Prince, R. Richter, R. Moshammer, T. Pfeifer, L. S. Cederbaum and M. Mudrich, *Phys. Rev. Lett.*, 2016, **116**, 203001.
3 A. C. LaForge, M. Shcherbinin, F. Stienkemeier, R. Richter, R. Moshammer, T. Pfeifer and M. Mudrich, *Nat. Phys.*, 2019, **15**, 247–250.
4 M. Shcherbinin, A. C. LaForge, M. Hanif, R. Richter and M. Mudrich, *J. Phys. Chem. A*, 2018, **122**, 1855–1860.
5 C. P. Schulz, P. Claas, D. Schumacher and F. Stienkemeier, *Phys. Rev. Lett.*, 2004, **92**, 013401.
6 A. Przystawik, S. Göde, T. Döppner, J. Tiggesbäumker and K.-H. Meiwes-Broer, *Phys. Rev. A: At., Mol., Opt. Phys.*, 2008, **78**, 021202.
7 M. Lasserus, D. Knez, F. Lackner, M. Schnedlitz, R. Messner, D. Schennach, G. Kothleitner, F. Hofer, A. W. Hauser and W. E. Ernst, *Phys. Chem. Chem. Phys.*, 2019, **21**, 21104–21108.
8 L. An der Lan, P. Bartl, C. Leidlmair, H. Schöbel, R. Jochum, S. Denifl, T. D. Märk, A. M. Ellis and P. Scheier, *J. Chem. Phys.*, 2011, **135**, 044309.
9 C. C. Wang, O. Kornilov, O. Gessner, J. H. Kim, D. S. Peterka and D. M. Neumark, *J. Phys. Chem. A*, 2008, **112**, 9356–9365.
10 L. Ben Ltaief, M. Shcherbinin, S. Mandal, S. R. Krishnan, A. C. LaForge, R. Richter, S. Turchini, N. Zema, T. Pfeifer, E. Fasshauer, N. Sisourat and M. Mudrich, *J. Phys. Chem. Lett.*, 2019, **10**, 6904–6909.
11 M. Mudrich, A. C. LaForge, A. Ciavardini, P. O'Keeffe, C. Callegari, M. Coreno, A. Demidovich, M. Devetta, M. D. Fraia, M. Drabbels, P. Finetti, O. Gessner, C. Grazioli, A. Hernando, D. M. Neumark, Y. Ovcharenko, P. Piseri, O. Plekan, K. C. Prince, R. Richter, M. P. Ziemkiewicz, T. Möller, J. Eloranta, M. Pi, M. Barranco and F. Stienkemeier, *Nat. Commun.*, 2020, **11**, 112.
12 P. O'Keeffe, P. Bolognesi, M. Coreno, A. Moise, R. Richter, G. Cautero, L. Stebel, R. Sergo, L. Pravica, Y. Ovcharenko and L. Avaldi, *Rev. Sci. Instrum.*, 2011, **82**, 033109.
13 M. Shcherbinin, A. C. LaForge, V. Sharma, M. Devetta, R. Richter, R. Moshammer, T. Pfeifer and M. Mudrich, *Phys. Rev. A*, 2017, **96**, 013407.
14 F. Stienkemeier and K. K. Lehmann, *J. Phys. B: At., Mol. Opt. Phys.*, 2006, **39**, R127.
15 J. P. Toennies and A. F. Vilesov, *Angew. Chem., Int. Ed.*, 2004, **43**, 2622–2648.
16 B. Dick, *Phys. Chem. Chem. Phys.*, 2014, **16**, 570–580.
17 M. Joppien, R. Karnbach and T. Möller, *Phys. Rev. Lett.*, 1993, **71**, 2654–2657.
18 N. Halberstadt and K. C. Janda, *Chem. Phys. Lett.*, 1998, **282**, 409–412.
19 J. Fennelly and D. Torr, *At. Data Nucl. Data Tables*, 1992, **51**, 321–363.
20 J. Kim and W. Huntress, *Int. J. Mass Spectrom. Ion Phys.*, 1975, **16**, 451–454.
21 P. Duffy, S. Clark, C. Brion, M. Casida, D. Chong, E. Davidson and C. Maxwell, *Chem. Phys.*, 1992, **165**, 183–199.
22 K. Ohno, H. Mutoh and Y. Harada, *J. Am. Chem. Soc.*, 1983, **105**, 4555–4561.
23 Y. Ono and C. Y. Ng, *J. Chem. Phys.*, 1982, **77**, 2947–2955.
24 Y. Ono and C. Y. Ng, *J. Am. Chem. Soc.*, 1982, **104**, 4752–4758.
25 M. Briant, E. Mengesha, M.-A. Gaveau, B. Soep, J.-M. Mestdagh and L. Poisson, *Phys. Chem. Chem. Phys.*, 2018, **20**, 2597–2605.
26 T. Stein, B. Bandyopadhyay, T. P. Troy, Y. Fang, O. Kostko, M. Ahmed and M. Head-Gordon, *Proc. Natl. Acad. Sci. U. S. A.*, 2017, **114**, E4125–E4133.
27 A. Kautsch, M. Koch and W. E. Ernst, *Phys. Chem. Chem. Phys.*, 2015, **17**, 12310–12316.
28 U. Henne and J. P. Toennies, *J. Chem. Phys.*, 1998, **108**, 9327–9338.
29 T. Horio, T. Hatamoto, S. Maeda, N. Kishimoto and K. Ohno, *J. Chem. Phys.*, 2006, **124**, 104308.
30 D. Buchta, S. R. Krishnan, N. B. Brauer, M. Drabbels, P. O'Keeffe, M. Devetta, M. Di Fraia, C. Callegari, R. Richter and M. Coreno, *et al.*, *J. Chem. Phys.*, 2013, **139**, 084301.
31 M. C. Wells and R. R. Lucchese, *J. Chem. Phys.*, 1999, **111**, 6290–6299.
32 D. S. Peterka, A. Lindinger, L. Poisson, M. Ahmed and D. M. Neumark, *Phys. Rev. Lett.*, 2003, **91**, 043401.
33 O. Kornilov, C. C. Wang, O. Bünermann, A. T. Healy, M. Leonard, C. Peng, S. R. Leone, D. M. Neumark and O. Gessner, *J. Phys. Chem. A*, 2010, **114**, 6350.
34 O. Bünermann, O. Kornilov, S. R. Leone, D. M. Neumark and O. Gessner, *IEEE J. Sel. Top. Quantum Electron.*, 2012, **18**, 308–317.